Atmospheric
Chemistry
and Physics
Discussions

Annual variation in precipitation δ^2H reflects vapor source region at Barrow, AK

Annie L. Putman[1,2], Xiahong Feng[1], Leslie J. Sonder[1], and Eric S. Posmentier[1]

[1]Department of Earth Sciences, Dartmouth College, Hanover, NH, USA.
[2]Department of Geology & Geophysics, University of Utah, Salt Lake City, UT, USA.

Correspondence to: Annie Putman (putmanannie@gmail.com)

Abstract. Interpretation of variability in precipitation stable isotopic ratios often relies exclusively on empirical relationships to meteorological variables (e.g., temperature) at the precipitation site. Because of the difficulty of unambiguously determining the vapor source region(s), relatively fewer studies consider evaporation and transport conditions. Increasing accessibility of Lagrangian air parcel tracking programs now allows for an integrated look at the relationship between the precipitation isotope

5 ratios and the evolution of moist air masses. In this study, 70 precipitation events occurring between January 2009 and March 2013 at Barrow, AK, USA, were analyzed for δ^2H and deuterium excess. For each precipitation event, vapor source regions were identified with the Lagrangian air parcel tracking program, HYSPLIT, in back-cast mode. The results show that the vapor source region migrated annually with the most distal (proximal) and southerly (northerly) vapor source regions occurred during the winter (summer). This may be linked to equatorial expansion and poleward contraction of the Polar circulation cell and the

10 extent of Arctic sea ice cover. Annual cycles of vapor source region latitude and δ^2H in precipitation were in phase; depleted (enriched) δ^2H values were associated with winter (summer) and distal (proximal) vapor source regions. Precipitation δ^2H responded to variation in vapor source region as reflected by significant correlations between δ^2H with the following three parameters: 1) total cooling between lifted condensation level and precipitating cloud at Barrow, $\Delta\bar{T}_{cool}$, 2) the meteorological conditions at the evaporation site quantified by 2 m dew point, $\bar{T}_d$, and 3) whether the transport crossed the Brooks and/or

15 Alaskan ranges, expressed as a Boolean variable, mtn. These three variables explained 52 % of the variance (p <0.001) in precipitation δ^2H with a sensitivity of -3.25 $\pm$ 0.57 ‰ °C^{-1} (p < 0.001) to $\Delta\bar{T}_{cool}$, 3.80 $\pm$ 0.78 ‰ °C^{-1} (p < 0.001) to T$_d$, and 34.29 $\pm$ 11.05 ‰ (p = 0.0028) depletion when mtn is true. The magnitude of each effect on isotopic composition also varied with vapor source region proximity. For storms with proximal vapor source regions (where $\Delta\bar{T}_{cool}$ <7 °C), $\Delta\bar{T}_{cool}$ explained 26 % of the variance in δ^2H, $\bar{T}_d$ alone accounted for 48 %, while mtn explained 5 %. For storms with distal vapor sources

20 ($\Delta\bar{T}_{cool}$ >7°C), $\Delta\bar{T}_{cool}$ explained 13 %, $\bar{T}_d$ explained only 10 %, and mtn explained 24 %. The deuterium excess annual cycle lagged by 2-3 months the δ^2H cycle, so the direct correlation between the two variables is weak. Neither vapor source sea surface temperature, nor vapor source relative humidity, nor a linear combination of the two, was a statistically significant predictor of precipitation deuterium excess. Vapor source region $\bar{T}_d$ explained 24 % of variance in deuterium excess, (-0.53 $\pm$ 0.12 ‰ °C^{-1}, p < 0.001). The patterns in our data suggest that on an annual scale, isotopic ratios of precipitation at Barrow

25 may respond to changes in the southerly extent of the Polar circulation cell. We expect isotopes to respond similarly for longer-term climate-induced changes to the mean position of meridional circulation features, and expect that the most of the variation

Atmospheric
Chemistry
and Physics
Discussions

Open Access

in isotopes measured in ice cores and other long term records are driven by changes in circulation, instead of fluctuations in local temperature.

1 Introduction

Changes to spatial patterns of water vapor transport and precipitation are an important component of incipient climate change (Santer et al., 2007; Marvel and Bonfils, 2013). The Arctic exhibits a particularly strong hydrologic response, including a notable increase in Arctic precipitation (Min et al., 2008; Bintanja and Selten, 2014; Kopec et al., 2016). Current and future changes in the hydrologic cycle may impact fresh water resources, natural disasters, and earth's radiation balance due to changes in timing, extent, and duration of snow or cloud cover (Liu et al., 2012).

Like changes in the timing or amount of precipitation, changes in the relative abundance of heavy-isotope substituted water molecules in precipitation (e.g., $^1H_2^{16}O$ vs. $^1H_2^{18}O$ and $^1H^2H^{16}O$) may reflect effects of changing climate on the hydrologic cycle. Historically, researchers have measured the isotopic ratios of precipitation on monthly or longer timescales and attempted to explain the temporal, altitude, and latitude variation of the isotopic ratios (Cappa et al., 2003; Rindsberger et al., 1983; Liu et al., 2010). Empirical analysis has focused on weather and climate conditions at the precipitation site (Dansgaard et al., 1969). Models developed to understand the spatial and temporal variability of water stable isotopes include evaporation and Rayleigh distillation models (Merlivat and Jouzel, 1979; Jouzel and Merlivat, 1984), models examining the balance of vertical mixing and meridional advection (Hendricks et al., 2000; Noone, 2008), and isotope-enabled general circulation models (GCMs) (e.g., Yoshimura et al., 2008; Dee et al., 2015; Jouzel et al., 1987).

Until recently, few isotope models considered meteorological conditions at the vapor source, in part because the evaporation site could not be unambiguously identified. Not knowing the vapor source prevents a comprehensive examination of the full vapor history. Recently developed Lagrangian air parcel tracking programs with quantitative source and trajectory meteorology enabled estimation of evaporation sites and thus have become a useful tool for interpreting precipitation isotope ratios (Ichiyanagi and Yamanaka, 2005; Strong et al., 2007; Treble et al., 2005; Sodemann et al., 2008b; Good et al., 2014; Wang et al., 2013).

The objective of this study is to understand how source and trajectory meteorology contribute to event-scale variations in the precipitation isotopic ratios and how such contributions vary over time (e.g., seasonally). To do this, we investigate the isotopic ratios of precipitation from event-scale sampling at Barrow, Alaska, USA. Barrow is one of nine sites that comprise the pan-Arctic Isotopic Investigation of Sea Ice and Precipitation in the Arctic Climate System campaign (iisPACS, (Feng, 2011)). This work utilizes intensive observations at Barrow under the Atmospheric Radiation Monitoring (ARM) program. Specifically, we use millimeter wavelength cloud radar (MMCR) to identify the precipitating clouds' altitude and rate of condensation to initialize Lagrangian air parcel tracking. Using direct cloud observations means that the backward trajectories are initiated at the appropriate time and from a distribution of altitudes representative of the actual heights of condensation. Such an initial distribution of air parcels is unique to our study. We distribute air parcels in proportion to the condensation rate, so that for a given event, each air parcel represents an equal amount of the precipitated water (Putman et al., 2015).

Atmospheric
Chemistry
and Physics
Discussions

This simplifies calculating the average vapor source, transport, and condensation conditions which we use to interpret the observed precipitation isotope ratios. Although this research focuses on precipitation data from a single location, the results link circulation to the precipitation isotope systematics of the sea-ice-sensitive high latitudes.

2 Methods

5 Event-scale precipitation samples were collected from 70 precipitation events at Barrow, AK, between January 2009 and April 2013. Below we describe methods for sample collection and measurement of δ^2H and δ^{18}O of precipitation, identification of vapor source regions, and characterization of evaporation and transport conditions using meteorological data from the source regions.

2.1 Sample collection and isotopic analysis

10 The sampling equipment was installed on a skydeck within the North Slope of Alaska facility of the Atmospheric Radiation Measurement (ARM) program. If the precipitation was rain, a rain funnel was used to collect the sample. If the precipitation was snow, the fresh snow was scooped into a plastic bag from a designated surface on the skydeck. The collection surface was five meters above the ground on the tower, ensuring minimal contribution of windblown snow from previous events. Samples were gathered less than 24 hours after the event ended. Liquid samples were stored in tightly sealed 30 mL Nalgene bottles and
15 shipped in batches to the Stable Isotope Laboratory at Dartmouth College. When not in transit, samples were refrigerated.

Upon arrival at Dartmouth the samples were prepared for analysis of hydrogen and oxygen isotopic ratios with a Delta Plus XL Isotope Ratio Mass Spectrometer (IRMS). For hydrogen measurements, the IRMS was connected to an HDevice reduction furnace: a reactor tube filled with a volumetric 1:1 mix of 100 mesh and 300 mesh chromium powder and set at 850 °C. One μL of sample was injected into the HDevice, and the water was allowed to react for two minutes in the hot chromium chamber,
20 reducing to hydrogen gas, which was then introduced to the dual inlet system of the mass spectrometer and measured by the IRMS. For oxygen isotope measurements, the IRMS was coupled to a GasBench. A 500 μL aliquot of liquid sample was placed in a vial, flushed with a mixture of 0.3 % CO_2 in helium, and allowed to equilibrate for at least 18 hours at 25 °C. The isotopic ratios of the CO_2 were measured by the IRMS. For both the oxygen and hydrogen measurements, the measured value was converted to the water-isotope equivalent by calibration with known standards. Isotopic ratios (^{2}H/^{1}H and ^{18}O/^{16}O),
25 are reported in delta notation: the deviation from the international standard VSMOW on the VSMOW-SLAP scale, defined as $\delta = [\frac{R_{SA} - R_{ST}}{R_{ST}}]$, where $R_{SA\,or\,ST} = \frac{^2[H]}{^1[H]}\,or\,\frac{[^{18}O]}{[^{16}O]}$. SA and ST indicate sample and standard, respectively. The uncertainties of the reported values are within $\pm$ 0.5 and $\pm$ 0.1 ‰ (one standard error) for δ^2H and δ^{18}O respectively.

2.2 Back trajectories

Back trajectories were performed using the air parcel tracking program HYSPLIT (Draxler, 1999; Draxler and Hess, 1997,
30 1998; Stein et al., 2015). To obtain a representative view of the vapor source region, the condensing air above Barrow, AK was subdivided into 1000 air parcels, each representing an equal amount of the condensing water. The height of each air parcel

will be referred to as the 'air parcel arrival height'. Each of the 1000 air parcels was tracked backward in time for 10 days (240 hours). A vapor source was declared the first time that the trajectory of the air parcel sank below the free troposphere into the planetary boundary layer (PBL). Only trajectories that sank into the PBL over the ocean were considered; parcels that never sank into the PBL or those that sank below the PBL over land were ignored. These were about 71% of all trajectories initiated.

5   Back trajectory analysis was performed for selected dates and times that most closely matched the occurrence of the precipitation events. The dates and times were chosen based on a combination of sampling records, surface analysis maps of Alaska available through the National Center for Environmental Prediction, and the returns of the millimeter wavelength cloud radar (MMCR) (Johnson and Jensen, 1996; Bharadwaj et al., 2011). On the date of precipitation, back trajectory start times were selected for maximum precipitation intensity as indicated by the MMCR. Because the gridded meteorological files used for

10   tracing the back trajectories had three-hour resolution, the starting time chosen represented average conditions over a three-hour period. If precipitation lasted for more than three hours, the most temporally homogeneous three-hour time window was selected, with preference for the middle of the event.

The method for selecting where the air parcels began their back trajectories is described in full in Putman et al. (2015). Briefly, returns of the reflectivity and Doppler vertical velocity (Holdridge et al., 1994; Regional Climate Center, 2012; John-

15   son and Jensen, 1996; Bharadwaj et al., 2011) from the MMCR were processed with algorithms developed by Zhao and Garrett (2008) to estimate the precipitation rate profile (g m^{-2} s^{-1}) as a function of height. The precipitation rate profile was differentiated with respect to height, yielding the condensation rate profile (g m^{-3} s^{-1}) and then subdivided into the aforementioned 1000 air parcels.

At both the vapor source region and the air parcel initiation altitude above the precipitation site, the meteorological data

20   for our analysis came from the Global Data Assimilation System (GDAS) reanalysis gridded dataset. At the vapor source, we extracted the 2 m relative humidity and 2 m air temperature. Sea surface temperature data for the deuterium excess analysis came from the NOAA gridded sea surface temperature dataset (NOAA/OAR/ESRL PSD at Boulder Colorado USA, 2013). At the condensation site, we extracted from GDAS the air temperature at each height containing an air parcel.

2.3 Calculation of $\bar{T}_d$, $\Delta\bar{T}_{cool}$ and mtn

25   To quantify the relationship between the vapor source region and the isotopic composition of precipitation, we used three physically based metrics: the average amount of cooling during air parcel transport $\Delta\bar{T}_{cool}$, the average dew point (evaporation conditions) at the vapor source region $\bar{T}_d$, and the presence or absence of mountains along the transport path mtn. The first two metrics were calculated from the meteorological data at the vapor source and precipitation site. The third, a Boolean variable, was assigned based on the air parcel trajectory.

30   The portion of the total air parcel cooling that produced condensation, ΔT_{cool}, represents the magnitude of Rayleigh distillation along the trajectory (Sodemann et al., 2008b). For a given air parcel, we calculate ΔT_{cool} as the difference between the temperature at the air parcel lifted condensation level (LCL) above the source region T_{LCL}, and the condensation temperature,

Atmospheric
Chemistry
and Physics

EGU

Discussions

Open Access

T_c, at the air parcel arrival height above Barrow, AK, i.e.,

$$\Delta T_{cool} = T_{LCL} - T_c \tag{1}$$

The temperature at the LCL, T_{LCL}, was determined by finding the altitude where the specific humidity Q, of the surface air parcel equaled the saturation specific humidity Q_{sat}. To calculate Q_{2m}, the 2 m temperature T_{2m}, fractional relative humidity

5 h_{2m}, pressure P_{2m}, were combined as in Equation 2. The same was done for an array of elevations z, where h_z was assumed to be 1, T_z was calculated from the dry adiabatic lapse rate (-9.8 °C km^{-1}), and P_z was calculated as in Equation 3. Thus T_{LCL} was T_z where $Q_{sat,z}$ equaled Q_{2m}.

$$Q = \frac{3270h}{P} 2^{\frac{T}{10}} \tag{2}$$

$$P(z) = 1013.25[1 - (2.25577 * 10^{-5})z]^{5.25588} \tag{3}$$

10 ΔT_{cool} was calculated individually for each of the 1000 trajectories in an event. We report the mean of all trajectories that were traced to the marine PBL, $\Delta \bar{T}_{cool}$, as characteristic of the event.

We used the vapor source 2 m dew point T_d, to represent the evaporation conditions at the vapor source region. T_d depends on the specific humidity of saturated air at the sea surface and on the amount of dry air from aloft that has subsided and mixed into low altitude air. The relative proportions of the saturated surface air and unsaturated subsiding air determine the properties

15 of the marine PBL. This makes T_d a useful indicator of integrated evaporation conditions at the vapor source. We approximate T_d with the 2 m air temperature, T_{2m}, and relative humidity, h_{2m}, using the following (Stull, 2015)

$$T_d = T_{2m} + 10 * log_2(h_{2m}) \tag{4}$$

T_d was calculated for the vapor source indicated by each of the 1000 trajectories that were traced to the marine PBL, and the mean of the 1000 T_d values is reported as a single value, $\bar{T}_d$, characteristic of the event.

20 Vapor originating in the Gulf of Alaska typically must be transported over the Alaska and Brooks Ranges to contribute to precipitation at Barrow, whereas vapor originating anywhere in the Arctic Ocean, Bering Strait, or western North Pacific typically does not encounter major orographic obstacles during its transport to Barrow. The orographic effect on isotope ratios of precipitation was quantified with a Boolean variable, 'mtn': defined as whether (1) or not (0) most air parcels crossed the Alaskan and/or Brooks ranges during transport to Barrow. The value of mtn was assigned based on the general pattern of

25 transport for the event, not to individual trajectories.

Atmospheric
Chemistry
and Physics
Discussions
Open Access
EGU

3 Results and discussion

In this section we discuss the vapor source annual cycle, and statistical relationships between the isotopic composition of precipitation, vapor source region, and the variables ($\Delta \bar{T}_{cool}$, $\bar{T}_d$, and mtn) that characterize the relationship of vapor source and transport to the isotope values measured at Barrow, AK.

3.1 Vapor source region annual cycle

The vapor source regions for precipitation at Barrow change seasonally (Figure 1). Vapor fueling winter (December, January, February) precipitation originated furthest south, typically in the Gulf of Alaska, and for most winter events, trajectories crossed the Alaskan and Brooks Ranges. In spring (March, April, May) the vapor for roughly half the precipitation events came from the North Pacific and traveled over the mountain ranges, as in winter. The vapor for the remaining precipitation events generally came from the southwest of Barrow, from Bering Strait and Chukchi Sea. Vapor source regions for summer (June, July and August) precipitation were the most northerly, typically the Chukchi Sea or Bering Strait. Synoptic systems moving counterclockwise around the Arctic Ocean characterized summer air parcel transport. In fall (September, October, November), vapor also came from the Chukchi and Beaufort seas, but with air parcel transport from the east to Barrow, the reverse of the spring and summer parcel transport patterns. The Gulf of Alaska provided vapor for a few fall events, with air parcel transport over the Brooks and/or Alaskan mountain ranges, as in winter.

In association with the latitudinal variation in the vapor source region, the temperature difference along the trajectory $\Delta \bar{T}_{cool}$ and vapor source dew point $\bar{T}_d$ also varied (Figure 2). The mean latitude of the vapor source region $\bar{V}_{Lat}$ and $\Delta \bar{T}_{cool}$ varied inversely, with more cooling being associated with lower $\bar{V}_{Lat}$, i.e. greater meridional transport. For any given season $\bar{T}_d$ was warmer in the south, and cooler in the north. There are also seasonal differences; at any latitude the dew point, $\bar{T}_d$, was warmer in summer and cooler in winter.

The migration of the mean latitude of the vapor source region is tied in two ways to the change in solar insolation in the northern hemisphere. Decreased solar insolation during winter drives expansion of the northern Polar circulation cell and increases sea ice cover. Increased sea ice cover diminishes the vapor contributions of the Arctic Ocean, allowing for enhanced representation of southerly vapor sources. Increased summer insolation drives poleward contraction of the circulation cell and diminishes sea ice coverage, such that the average vapor source area migrates north. Feng et al. (2009) documented similar vapor source migration over a much larger scale, in association with the annual north-south migration of circulation cells.

The latitudinal extent of the Polar circulation cell likely varies over time scales ranging from interannual to millenial, causing changes to vapor sources and the Arctic hydrologic cycle on corresponding time scales. Marvel and Bonfils (2013) suggest that a poleward displacement of circulation cells is already occurring due to recent climate change. Southward migration of the polar cell during the last glacial maximum has been documented by Feng et al. (2007). Changes in the isotopic composition of precipitation resulting from systematic vapor source migrations associated with changing climate allow for interpretation of long-term isotopic records in terms of changes in atmospheric circulation.

3.2 The influence of vapor source on precipitation δ^2H

Figure 3 shows that the measured δ^2H values of the 70 precipitation events fall between -280‰ and -50‰, with a pattern of summer enrichment and winter depletion that follows the well-established annual cycle for high latitudes (Feng et al., 2009). The local meteoric water line (with 95 % confidence intervals), $\delta^2 H = 7.78(\pm0.12)\delta^{18}O + 7.18(\pm2.61)$, is statistically

5   distinguishable from the global meteoric water line ($\delta^2 H = 8\delta^{18}O + 10$). Figure 3 also shows the interannual, seasonal and event-scale variability captured by the dataset. The average annual cycle of the precipitation δ^2H is in phase with the mean latitude of the vapor source, as shown in Figure 4.

    The phase relationship between δ^2H and the north-south migration of the vapor source region occurs because the vapor source region governs three critical metrics that affect the δ^2H of precipitation: 1) the temperature difference between vapor

10   source region and precipitation site, quantified by air parcel cooling $\Delta\bar{T}_{cool}$ (Figure 2), 2) the evaporation conditions, quantified in this work by $\bar{T}_d$ (Figure 2), and 3) the mean air parcel transport path (Figure 5). A linear combination of $\Delta\bar{T}_{cool}$, $\bar{T}_d$, and mtn statistically represents the event-scale variation in δ^2H with an R^2 value of 0.52 (p < 0.001). Table 1 contains the correlation slopes (β), p-values, and the unique variance explained by each variable. Below we discuss the physical mechanisms that may explain the influence of each of these metrics on δ^2H.

15   In contrast with previous assumptions that local (precipitation site) surface temperature is a metric for Rayleigh distillation (e.g., Dansgaard, 1964), our study compares δ^2H with $\Delta\bar{T}_{cool}$, $\bar{T}_d$ and mtn. Using these metrics instead of local surface temperature allows us to circumvent two restrictive assumptions. First, we do not assume that δ^2H has a spatially and temporally stationary relationship to local temperature. Bowen (2008) demonstrated that this assumption does not hold. Rather, because meridional temperature gradients are an important driver of the isotope-temperature sensitivity (Hendricks et al., 2000), when

20   the meridional temperature gradient fluctuates, a quantity that $\Delta\bar{T}_{cool}$ captures, the sensitivity of δ^2H to local temperature also fluctuates. Likewise, the presence of mountains along the vapor transport path will deplete the isotope ratio of the precipitation relative to an over-ocean transport, all other meteorological conditions being equivalent. The second restriction associated with using local surface temperature as a metric of Rayleigh distillation assumes that vapor for all precipitation events comes from a single, homogeneous source. It requires that the δ^2H of the water vapor, and thus the initial condensate, is constant in space

25   and time. However, global measurements from the Tropospheric Emissions Spectrometer (Good et al., 2015) indicate that the vapor in the planetary boundary layer over the ocean varies with space and season, confirming previous land and ship measurements (e.g., Steen-Larsen et al., 2014; Kurita, 2011; Uemura et al., 2008). Likewise, our results indicate that vapor may come from a heterogeneous source region or variety of source regions (Figure 1) and the initial condensate, based on the evaporation conditions, should be expected to vary. The effect of a meteorologically heterogeneous source region is captured

30   by $\bar{T}_d$.

    As expected, $\Delta\bar{T}_{cool}$ accounts for the largest proportion of variance in δ^2H (23%) among the explanatory variables. Our statistical correlation yields a sensitivity of -3.25‰ °C^{-1} for δ^2H with respect to $\Delta\bar{T}_{cool}$ (Table 1). Because Rayleigh distillation is considered the main source of spatial variation in δ^2H, comparison with the sensitivities calculated from a simple Rayleigh model contextualize our result. We determined condensation in a moist air parcel for both adiabatic decompression

and isobaric radiative cooling using equilibrium isotope fractionation factors from Majoube (1971). Because the association between precipitation δ^2H and $\Delta\bar{T}_{cool}$ during a Rayleigh process varies (Dansgaard, 1964), the sensitivity range for moist adiabatic cooling from 10 °C to -15 °C, with a lapse rate of -6.5 °C km^{-1}, ranges between -3.46 ‰ °C^{-1} to -5.45 ‰ °C^{-1}, while moist isobaric radiative cooling across the same temperature range yields sensitivities from -5.47 ‰ °C^{-1} to -7.88 ‰

5 °C^{-1}. The sensitivity exhibited by our data is just below the low end of the range determined for moist adiabatic cooling and was significantly lower than the range using isobaric cooling. The similarity between our data and the moist adiabatic model results suggest that moist adiabatic cooling was likely the dominant mechanism for precipitation during air parcel transport to Barrow, although scatter in the δ^2H data could also be due to variable contributions of radiative cooling. The relatively low observed sensitivity relative to the theoretical sensitivities may be explained by additions of vapor to air parcels during

10 poleward meridional transport, following the two-stream isentropic vapor source transport model (Noone, 2008).

Our multiple linear model attributes a substantial fraction of the variance in δ^2H to variations in $\bar{T}_d$ (17%). This is because source meteorological conditions control the δ^2H of the water evaporated from the ocean surface. Studies typically attribute variations in δ^2H values at the source to mean sea surface temperature $\bar{T}_{ss}$ and mean 2 m relative humidity $\bar{h}$, which affect the magnitudes of equilibrium and kinetic fractionation, respectively (Craig and Gordon, 1965). Assuming that $\bar{T}_{ss}$ influences

15 2 m air temperature, so that the two temperatures correlate spatially, we may use the 2 m dew point ($\bar{T}_d$) at the vapor source to combine the effects of $\bar{T}_{ss}$ and $\bar{h}_{2m}$. Either high $\bar{T}_{ss}$ or high $\bar{h}_{2m}$ results in high $\bar{T}_d$. Therefore, we expect $\bar{T}_d$ to be positively associated with δ^2H in the original vapor in an air parcel at the vapor source. This δ^2H signal at the source is then carried to the precipitation site. Differences in $\bar{T}_{2m}$ cause > 20 °C of the ~25 °C range we report for $\bar{T}_d$, whereas $\bar{h}_{2m}$ contributes 2-4 °C. The substantial difference between the vapor source $\bar{T}_d$ for Arctic compared with subtropical sources makes $\bar{T}_d$ a more useful

20 metric for characterizing the vapor source than either $\bar{T}_{ss}$ or $\bar{h}_{2m}$ alone.

Given the magnitude of variability in $\bar{T}_d$ attributed to temperature, the relationship of δ^2H to $\bar{T}_d$ should be comparable to the equilibrium fractionation relationship between δ^2H and $\bar{T}_{ss}$. For δ^2H relative to $\bar{T}_d$ we report a sensitivity of 3.80 ‰°C^{-1} (Table 1). In comparison, for $\bar{T}_{ss}$ between 0-25 °C, equilibrium fractionation as a function of temperature yields sensitivities between 1.1-1.6 ‰°C^{-1} (Majoube, 1971). The sensitivities have the same sign, indicating that warm evaporation temperatures

25 correlate with high vapor isotopic ratios. The sensitivity of δ^2H to $\bar{T}_d$ is 2 to 4 times that of δ^2H to $\bar{T}_{ss}$, meaning that equilibrium fractionation accounts for less than half of the sensitivity. Kinetic fractionation associated with variation in $\bar{h}_{2m}$ (e.g., entrainment of upper atmosphere air) may contribute some of the remaining sensitivity. Other factors that influence evaporation, such as wind speed and sea surface roughness (Merlivat and Jouzel, 1979) may have covaried spatially with $\bar{T}_d$ and influenced the reported sensitivity. Partitioning the effects of windspeed and surface roughness requires further investigation.

30 To reach Barrow, AK, air parcels originating in the Gulf of Alaska must cross the Alaska and/or Brooks Ranges, whereas air parcels from the Bering Strait or Chukchi Sea do not have to cross high topography. Our work shows that transport across mountain ranges resulted in significant δ^2H depletion in Barrow precipitation. Transport of vapor over mountain ranges occurred more frequently during cold months, when the Gulf of Alaska and North Pacific were the dominant vapor source regions. Since the vapor source location in winter is governed by the expansion of the Polar circulation cell, the projected northward

35 displacement of subtropical highs and the Polar front (Marvel and Bonfils, 2013) in a warming climate may be associated with

Atmospheric
Chemistry
and Physics
Discussions

a reduced amounts of vapor transported over the Alaskan and/or Brooks ranges during fall, winter and spring. Fewer events traveling over the Alaskan and/or Brooks ranges would correspond to a pronounced enrichment in measured δ^2H at Barrow during cold months.

To study the importance of $\bar{T}_d$ and mtn as explanatory variables with respect to cooling during transport ($\Delta\bar{T}_{cool}$), we divided our data into subgroups: $\Delta\bar{T}_{cool}$ <7 °C and $\Delta\bar{T}_{cool}$ >7 °C and recalculated the statistics. Table 2 summarizes the results. For the small $\Delta\bar{T}_{cool}$ subgroup, $\bar{T}_d$ explains almost half the variance in δ^2H (R^2 = 0.48) whereas for the large $\Delta\bar{T}_{cool}$ subgroup $\bar{T}_d$ explains very little variance (R^2 = 0.10). This difference implies enhanced isotopic modification over long trajectories. In contrast, the δ^2H values of the small $\Delta\bar{T}_{cool}$ subgroup are not well explained by the Boolean variable mtn (R^2 = 0.05), whereas mtn explains a quarter of the variability of the large $\Delta\bar{T}_{cool}$ subgroup (R^2 = 0.24). As expected, some variability in each subgroup is explained by $\Delta\bar{T}_{cool}$. The small $\Delta\bar{T}_{cool}$ subgroup, $\Delta\bar{T}_{cool}$ explained a quarter (R^2 = 0.26) of the variance in δ^2H, and for the large $\Delta\bar{T}_{cool}$ subgroup R^2 = 0.13.

Because the events with smallest $\Delta\bar{T}_{cool}$ tended to occur in summer, the strong relationship between $\bar{T}_d$ and δ^2H indicates that precipitation δ^2H in summer predominantly reflects variability in evaporation conditions. The strong relationship between mtn and the variation in δ^2H for large $\Delta\bar{T}_{cool}$ indicates that precipitation δ^2H in winter predominantly reflects whether most air parcels crossed the Alaska and/or Brooks mountain ranges. Notably, $\Delta\bar{T}_{cool}$ could significantly predict δ^2H for both long and short trajectory events, but explained less variance than expected, given the emphasis on Rayleigh distillation in isotope hydrology.

Among the simple regressions, almost half the variance in δ^2H for events with $\Delta\bar{T}_{cool}$ <7 °C was explained by $\bar{T}_d$. This is a notable result, as the isotope composition of the initial vapor is not emphasized to the same degree as Rayleigh distillation in isotope hydrology. There are two reasons why $\bar{T}_d$ may explain so much variance for short trajectory events. First, storm events with minimal cooling during air parcel transport typically originated close to Barrow in the Arctic Ocean. A smaller vapor source area predicts less variation in T_d among air parcels: a homogeneous source. We quantify this effect by examining the distribution of within-storm $\bar{T}_d$ standard deviations ($\sigma\bar{T}_d$) for the short and long trajectory event subsets (Figure 6). Short trajectory ($\Delta\bar{T}_{cool}$ <7 °C) events had a median $\sigma\bar{T}_d$ of 2.87 °C, which was smaller than the long trajectory ($\Delta\bar{T}_{cool}$ >7 °C) median $\sigma\bar{T}_d$ of 5.44 °C. Less variability among air parcels in the short trajectory subset allowed the among-event relationship of δ^2H to $\bar{T}_d$ to emerge. Second, some of the variability in measured precipitation δ^2H may be caused by processes occurring during transport, such as radiative cooling, air mass mixing, and different degrees of mountain-induced rainout. The opportunity for these effects to impact the precipitation isotope value increases with increasing transport distance, obscuring the relationship of the precipitation δ^2H to the δ^2H of the initial vapor at the source and therefore to $\bar{T}_d$.

3.3 The influence of vapor source on deuterium excess

Deuterium excess (d-excess, or d) is often used to investigate conditions at vapor source regions such as T_{ss} and h that affect evaporation (Dansgaard, 1964). Empirical studies have linked marine boundary layer vapor deuterium excess ($d = \delta^2H - \delta^{18}O$) to T_{ss} and h (Uemura et al., 2008; Kurita, 2011; Steen-Larsen et al., 2014). These results agree qualitatively or semi-quantitatively with theoretical predictions (Merlivat and Jouzel, 1979; Craig and Gordon, 1965). However, in order for source

vapor d values to be preserved in precipitation, d must be conserved through condensation and post-condensation processes. This assumption may not be realistic. First, even simple equilibrium Rayleigh distillation does not yield constant d values in precipitation (Dansgaard, 1964). Second, non-equilibrium processes associated with snow formation may substantially alter d (Jouzel and Merlivat, 1984). Third, evaporation or sublimation under the cloud base and/or at the snow surface tends to

5   decrease d (Stichler et al., 2001).

Direct comparison of precipitation d to vapor source conditions via Lagrangian back trajectory vapor source estimation has produced complicated results. For example, Sodemann et al. (2008a) found that while the d of precipitation contains identifiable source information, it 'does not directly translate into the source region $\bar{T}_{ss}$'. In a study of vapor sources for precipitation in Antarctica, Wang et al. (2013) noted that the classical interpretation of measured d would predict that the highest average d

10   found at Dome Argus would correspond to the warmest (most northerly) vapor sources. However, precipitation at Dome Argus was linked to southerly vapor sources. The authors suggested the high d value was due to the vapor pressure deficit of dry air blowing off sea ice. Likewise Good et al. (2014) attributed the significant correlation between high d and source relative humidity (h) for precipitation collected at four northeast U.S. locations during Superstorm Sandy to oceanic evaporation into a dry continental air mass that was entrained into the superstorm.

15   Our study reveals a similarly inconclusive relationship between vapor source and event-scale precipitation d: d is not significantly predicted by $\bar{h}_{2m}$ (p = 0.36) but is significantly predicted by $\bar{T}_{ss}$ (p = 0.016), though the variance explained is 8 % and the sign of the coefficient is negative (Table 3), opposite of expectations. If d is regressed against both $\bar{T}_{ss}$ and $\bar{h}_{2m}$, the multiple regression is marginally significant (p = 0.051, not shown in Table 3) and explains 8 % of variance. The vapor source region dew point, $\bar{T}_d$, significantly predicts d (p <0.001) and explains a non-trivial portion of the variance (R^2 = 0.24), although

20   the sign of the regression coefficient is opposite of theoretical expectations.

Despite the apparent poor correlation between d and vapor source conditions, our dataset shows systematic seasonal variations. Figure 7 shows that d cycles annually with the maximum occurring in October or November, lagging the annual maximum of δ^2H by 2-3 months (or $\sim 90°$). This phase relationship explains the lack of linear association between d and $\bar{T}_{ss}$ and $\bar{h}_{2m}$ we report. Systematic seasonal variations in precipitation d occur in the Northern Hemisphere (Feng et al., 2009),

25   particularly in the Arctic (White et al., 1988; Johnsen et al., 1989; Kopec et al., 2016; Kurita, 2011). These studies suggest that the conditions producing d variation have systematic annual variations in their magnitude and relative importance.

4   Conclusions

The vapor source regions identified by HYSPLIT for storms at Barrow, AK, USA exhibit interannual, annual, and inter-event variability. Vapor comes from the North Pacific and Gulf of Alaska, the most southerly vapor source areas, in cold months when

30   the Polar circulation cell extends southward. Vapor comes from the Bering, Chukchi and Beaufort seas, the most northerly sources, in warm months when the Polar cell contracts northward. The cycle of winter depletion and summer enrichment exhibited by the δ^2H of the precipitation follows the annual changes in the latitude of the vapor source region, as a result of source region controls on evaporation, transport, and condensation conditions. A linear combination of the average vapor

Atmospheric
Chemistry
and Physics
Discussions

source region dew point ($\bar{T}_d$, β = 3.80 ‰ °C^{-1}), average cooling of the air parcels during transport ($\Delta\bar{T}_{cool}$, β = -3.25 ‰ °C^{-1}) and passage of air parcels over mountains or not (mtn, β = -34.29 ‰ when mtn = 1) explains 52 % of the event-scale variance in δ^2H. For the subset of events where $\Delta\bar{T}_{cool}$ was < 7 °C, $\bar{T}_d$ alone explained 48 % of the variance in δ^2H. For the subset of events where $\Delta\bar{T}_{cool}$ was > 7 °C, $\bar{T}_d$ did not significantly predict δ^2H, but mtn alone explained 24 % of the variance in δ^2H. Neither the average vapor source relative humidity, nor the average vapor source sea surface temperature, nor both combined, significantly explained the variations in deuterium excess, although a systematic seasonal variation with maximum d in October and minimum d in March was noted. The vapor source region dew point explained 24 % of the variance in d, though the sensitivity of d with respect to $\bar{T}_d$ was negative. Additional study is needed to understand among event variations in precipitation d.

Our study highlights how the variations in stable isotopes of precipitation can be interpreted in the context of the vapor source when precipitation is measured on an event-by-event basis. The mechanisms identified, most notably the north-south migration of the vapor source region in response to expansion and contraction of the Polar circulation cell, are expected to also operate on times scales longer than that of our study e.g., interannual, decadal, millenial, or glacial-interglacial. The associated precipitation isotopic response at a given site to the variability of the vapor source should be recorded in ice cores, lake sediments, pedogenic carbonates, and speleothems.

5 Data availability

The processed data used for this research is available as a supplement to the manuscript. Raw and partially processed results of the back trajectory runs may be obtained from Annie Putman (putmanannie@gmail.com).

Atmospheric
Chemistry
and Physics
Discussions

References

Bharadwaj, N., Widener, K., Nelson, D., Venkatesh, V., Lindenmaier, I., and Johnson, K.: KAZRGE 4-1-2011 to 4-1-2013, 71.323 N 156.609 W: North Slope Alaska (NSA) Central Facility, Barrow AK (C1), 2011.

Bintanja, R. and Selten, F. M.: Future increases in Arctic precipitation linked to local evaporation and sea-ice retreat, Nature, 509, 479–482, doi:10.1038/nature13259, 2014.

Bowen, G.: Spatial analysis of the intra-annual variation of precipitation isotope ratios and its climatological corollaries, J Geophys Res - Atmos, 113, doi:10.1029/2007JD009295, 2008.

Cappa, C. D., Hendricks, M. B., DePaolo, D. J., and Cohen, R. C.: Isotopic fractionation of water during evaporation, J Geophys Res, 108, 4525, doi:10.1029/2003JD003597, 2003.

Craig, H. and Gordon, L. I.: Deuterium and oxygen 18 variations in the ocean and marine atmosphere, in: Stable Isotopes in Oceanographic Studies and Paleotemperatures, p. 9, 1965.

Dansgaard, W.: Stable isotopes in precipitation, Tellus, 16, 436–468, doi:10.1111/j.2153-3490.1964.tb00181.x, 1964.

Dansgaard, W., S. J. Johnsen, J. M., and Langway, C. C.: One Thousand Centuries of Climatic Record from Camp Century on the Greenland Ice Sheet, Science, 166, 377–380, doi:10.1126/science.166.3903.377, 1969.

Dee, S., Noone, D., Buenning, N., Emile-Geay, J., and Zhou, Y.: SPEEDY-IER: A fast atmospheric GCM with water isotope physics, J Geophys Res - Atmos, 120, 73–91, doi:10.1002/2014JD022194, 2015.

Draxler, R. R.: HYSPLIT4 user's guide, Tech. Rep. ERL ARL-230D, NOAA Tech Memo, 1999.

Draxler, R. R. and Hess, G. D.: Description of the HYSPLIT4 modeling system, Tech. Rep. ERL ARL-224, NOAA Tech Memo, 1997.

Draxler, R. R. and Hess, G. D.: An overview of the HYSPLIT4 modeling system of trajectories, dispersion, and deposition., Aus Meteorol Mag, p. 295, 1998.

Feng, X.: Isotopic Investigation of Sea-ice and Precipitation in the Arctic Climate System, http://www.dartmouth.edu/~iispacs/, 2011.

Feng, X., Reddington, A. L., Faiia, A. M., Posmentier, E. S., Shu, Y., and Xu, X.: The changes in North American atmospheric circulation patterns indicated by wood cellulose, Geology, 35, 163–166, doi:10.1130/G22884A.1, 2007.

Feng, X., Faiia, A. M., and Posmentier, E. S.: Seasonality of isotopes in precipitation: A global perspective, J Geophys Res, 114, D08 116, doi:10.1029/2008JD011279, 2009.

Good, S., Mallia, D. V., Lin, J. C., and Bowen, G. J.: Stable Isotope Analysis of Precipitation Samples Obtained via Crowdsourcing Reveals the Spatiotemporal Evolution of Superstorm Sandy, PloS one, 9, e91 117, doi:10.1371/journal.pone.0091117, 2014.

Good, S., Noone, D., Kurita, N., Benetti, M., and Bowen, G.: D/H isotope ratios in the global hydrologic cycle, Geophys Res Lett, 42, 5042–5050, doi:10.1002/2015GL064117, 2015.

Hendricks, M. B., DePaolo, D. J., and Cohen, R. C.: Space and time variation of $\delta^{18}O$ and δD in precipitation: Can paleotemperature be estimated from ice cores?, Global Biogeochem Cy, 14, 851–861, doi:10.1029/1999GB001198, 2000.

Holdridge, D., Kyrouac, J., and Coulter, R.: SONDEWNPN 2009-01-01 to 2013-03-28, 71.323 N 156.609 W: North Slope Alaska (NSA) Central Facility, Barrow AK (C1), 1994.

Ichiyanagi, K. and Yamanaka, M. D.: Interannual variation of stable isotopes in precipitation at Bangkok in response to El Niño Southern Oscillation, Hydrol Process, 19, 3413–3423, doi:10.1002/hyp.5978, 2005.

Johnsen, S. J., Dansgaard, W., and White, J. W. C.: The origin of Arctic precipitation under present and glacial conditions, Tellus B, 41, 452–468, 1989.

Atmospheric
Chemistry
and Physics
Discussions

Johnson, K. and Jensen, M.: ARSCL1CLOTH 1-1-2009 to 4-1-2013, 71.323 N 156.609 W: North Slope Alaska (NSA) Central Facility, Barrow AK (C1), 1996.

Jouzel, J. and Merlivat, L.: Deuterium and Oxygen-18 in Precipitation: Modeling of the Isotopic Effects During Snow Formation, J Geophys Res, 89, 11 749–11 757, doi:10.1029/JD089iD07p11749, 1984.

5 Jouzel, J., Russell, G. L., Suozzo, R. J., Koster, R. D., White, J. W. C., and Broecker, W. S.: Simulations of the HDO and $H_2^{18}O$ atmospheric cycles using the NASA GISS general circulation model: The seasonal cycle for present-day conditions, journal=J Geophys Res - Atmos, volume=92, number=D12, pages=14739-14760, doi = 10.1029/JD092iD12p14739, 1987.

Kopec, B., Feng, X., Michel, F. A., and Posmentier, E.: Influence of sea ice on Arctic precipitation, PNAS, 113, 46–51, doi:10.1073/pnas.1504633113, 2016.

10 Kurita, N.: Origin of Arctic water vapor during the ice-growth season, Geophys Res Lett, 38, L02 709, doi:10.1029/2010GL046064, 2011.

Liu, J., Curry, J. A., H. Wang, M. S., and Horton, R. M.: Impact of declining Arctic sea ice on winter snowfall, PNAS, doi:10.1073/pnas.1114910109, 2012.

Liu, Z., Bowen, G. J., and Welker, J. M.: Atmospheric circulation is reflected in precipitation isotope gradients over the conterminous United States, J Geophys Res - Atmos, 115, D22 120, doi:10.1029/2010JD014175, 2010.

15 Majoube, M.: Oxygen-18 and deuterium fractionation between water and steam, J Chim Phys PCB, 68, 1423, 1971.

Marvel, K. and Bonfils, C.: Identifying external influences on global precipitation, PNAS, 110, 19 301–19 306, doi:10.1073/pnas.1314382110, 2013.

Merlivat, L. and Jouzel, J.: Global climatic interpretation of the deuterium-oxygen 18 relationship for precipitation, J Geophys Res - Oceans, 84, 5029–5033, doi:10.1029/JC084iC08p05029, 1979.

20 Min, S. K., Zhang, X., and Zwiers, F.: Human-Induced Arctic Moistening, Science, 320, 518–520, doi:10.1126/science.1153468, 2008.

NOAA/OAR/ESRL PSD at Boulder Colorado USA: NOAA OI SST V2 data, 2013.

Noone, D.: The influence of midlatitude and tropical overturning circulation on the isotopic composition of atmospheric water vapor and Antarctic precipitation, J Geophys Res - Atmos, 113, doi:10.1029/2007JD008892, 2008.

Putman, A., Posmentier, E. S., Faiia, A. M., Sonder, L. J., and Feng, X.: Verification of a novel method for identifying vapor sources using
25 air parcel back trajectories, in review, 2015.

Regional Climate Center, W.: Barrow WSO Airport (500546), 2012.

Rindsberger, M., Magaritz, M., Carmi, I., and Gilad, D.: The relation between air mass trajectories and the water isotope composition of rain in the Mediterranean Sea area, Geophys Res Lett, 10, 43–46, doi:10.1029/GL010i001p00043, 1983.

Santer, B. D., Mears, C., Wentz, F. J., Taylor, K. E., Gleckler, P. J., Wigley, T. M. L., Barnett, T. P., Boyle, J. S., Brüggemann, W., Gillett, N. P.,
30 Klein, S. A., Meehl, G. A., Nozawa, T., Pierce, D. W., Stott, P. A., Washington, W. M., and Wehner, M. F.: Identification of human-induced changes in atmospheric moisture content, PNAS, 104, 15 248–15 253, doi:10.1073/pnas.0702872104, 2007.

Sodemann, H., Masson-Delmotte, V., Schwierz, C., Vinther, B. M., and Wernli, H.: Interannual variability of Greenland winter precipitation sources: 2. Effects of North Atlantic Oscillation variability on stable isotopes in precipitation, J Geophys Res - Atmos, 113, D12 111, doi:10.1029/2007JD009416, 2008a.

35 Sodemann, H., Schwierz, C., and Wernli, H.: Interannual variability of Greenland winter precipitation sources: Lagrangian moisture diagnostic and North Atlantic Oscillation influence, J Geophys Res - Atmos, 113, D03 107, doi:10.1029/2007JD008503, 2008b.

Atmospheric
Chemistry
and Physics
Discussions

Open Access

Steen-Larsen, H., Sveinbjörnsdottir, A. E., Peters, A., Masson-Delmotte, V., Guishard, M., Hsiao, G., Jouzel, J., Noone, D., Warren, J., and White, J.: Climatic controls on water vapor deuterium excess in the marine boundary layer of the North Atlantic based on 500 days of in situ, continuous measurements, Atmos Chem Phys, 14, 7741–7756, doi:10.5194/acp-14-7741-2014, 2014.

Stein, A. F., Draxler, R. R., Rolph, G. D., Stunder, B. J. B., Cohen, M. D., and Ngan, F.: NOAA's HYSPLIT Atmospheric Transport and Dispersion Modeling System, B Am Meteorol Soc, 96, 2059–2077, doi:10.1175/BAMS-D-14-00110.1; 21, 2015.

Stichler, W., Schotterer, U., Fröhlich, K., Ginot, P., Kull, C., Gäggeler, H., and Pouyaud, B.: Influence of sublimation on stable isotope records recovered from high-altitude glaciers in the tropical Andes, J Geophys Res - Atmos, 106, 22 613–22 620, doi:10.1029/2001JD900179, 2001.

Strong, M., Sharp, Z. D., and Gutzler, D. S.: Diagnosing moisture transport using D/H ratios of water vapor, Geophys Res Lett, 34, L03 404, doi:10.1029/2006GL028307, 2007.

Stull, R.: Practical Meteorology: An Algebra-based Survey of Atmospheric Science, Dept. of Earth, Ocean & Atmospheric Sciences University of British Columbia, Vancouver, BC, Canada, 3rd edn., http://www.eos.ubc.ca/books/Practical_Meteorology/, 2015.

Treble, P. C., Budd, W. F., Hope, P. K., and Rustomji, P. K.: Synoptic-scale climate patterns associated with rainfall $\delta^{18}O$ in southern Australia, J Hydrol, 302, 270–282, doi:10.1016/j.jhydrol.2004.07.003, 2005.

Uemura, R., Matsui, Y., Yoshimura, K., Motoyama, H., and Yoshida, N.: Evidence of deuterium excess in water vapor as an indicator of ocean surface conditions, J Geophys Res - Atmos, 113, D19 114, doi:10.1029/2008JD010209, 2008.

Wang, Y., Sodemann, H., Hou, S., Masson-Delmotte, V., Jouzel, J., and Pang, H.: Snow accumulation and its moisture origin over Dome Argus, Antarctica, Clim Dynam, 40, 731–742, doi:10.1007/s00382-012-1398-9, 2013.

White, J. W. C., Johnsen, S. J., and Dansgaard, W.: The origin of Arctic precipitation as deduced from its deuterium excess, Ann Glaciol, 10, 219–220, 1988.

Yoshimura, K., Kanamitsu, M., Noone, D., and Oki, T.: Historical isotope simulation using Reanalysis atmospheric data, J Geophys Res - Atmos, 113, doi:10.1029/2008JD010074, 2008.

Zhao, C. and Garrett, T. J.: Ground-based remote sensing of precipitation in the Arctic, J Geophys Res, 115, 1, doi:10.1029/2007JD009222, 2008.
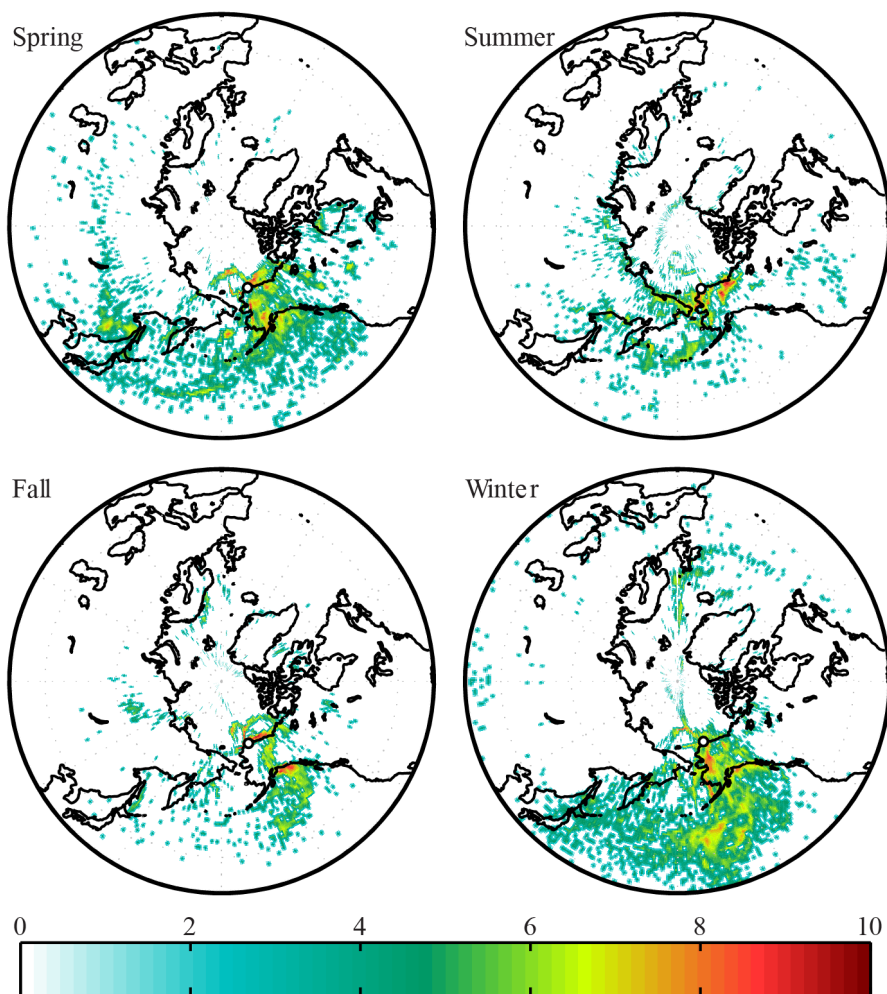
Figure 1. Spatial distribution of the vapor source region by season. Color indicates the relative frequency that a pixel was identified by HYSPLIT as a vapor source. Red indicates the most frequent vapor source for a given season, whereas dark blue indicates few air parcels were traced to that location. Because different numbers of events occurred in each season, each season's color scale is normalized to the total number of air parcels tracked during that season.
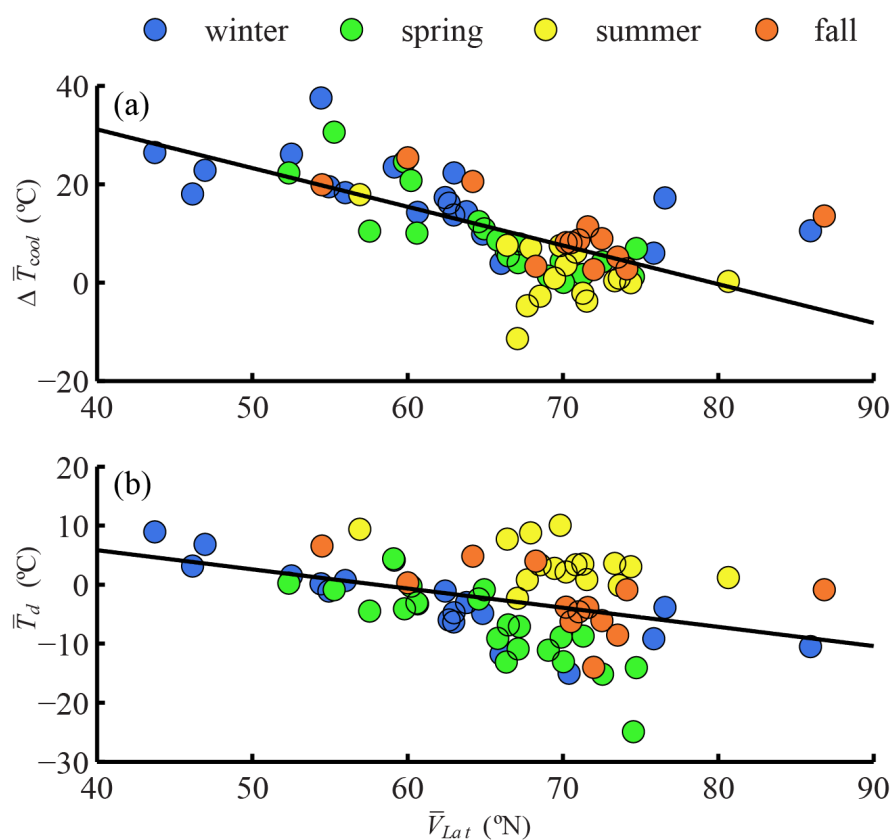
Figure 2. (a) Mean vapor source region latitude, $\bar{V}_{Lat}$, and mean air parcel cooling during transport, $\Delta\bar{T}_{cool}$, covary. (b) Mean vapor source region latitude, $\bar{V}_{Lat}$, and dew point, $\bar{T}_d$, also covary. Both $\Delta\bar{T}_{cool}$ and $\bar{T}_d$ influence the δ^2H of precipitation at Barrow. Scatter from best fit line is due, in part, to seasonal variation in latitudinal temperature gradients and vapor source conditions.
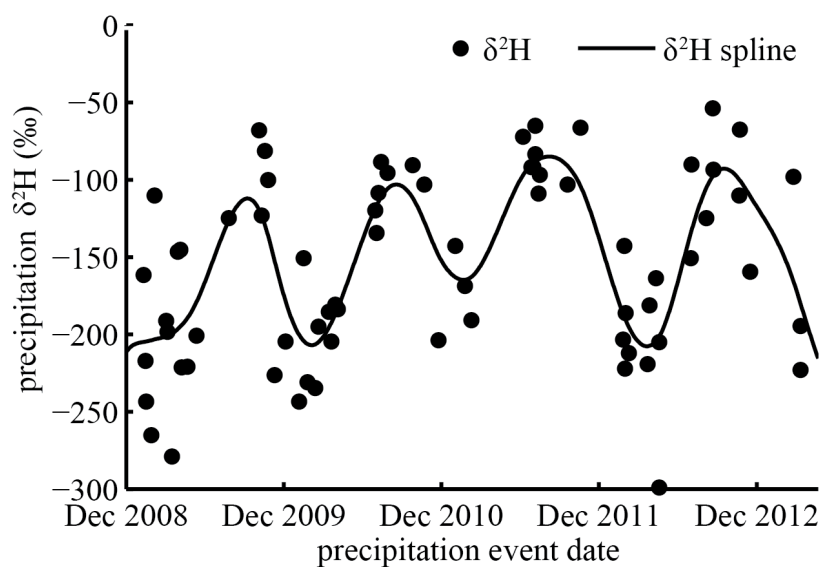
Figure 3. The δ^2H measured in precipitation at Barrow, AK, exhibited variability on interannual, annual and event time scales. Annual variability is the greatest, with enrichment corresponding roughly to the warmest months (June, July, August), and depletion corresponding roughly to the coldest months (December, January, February).
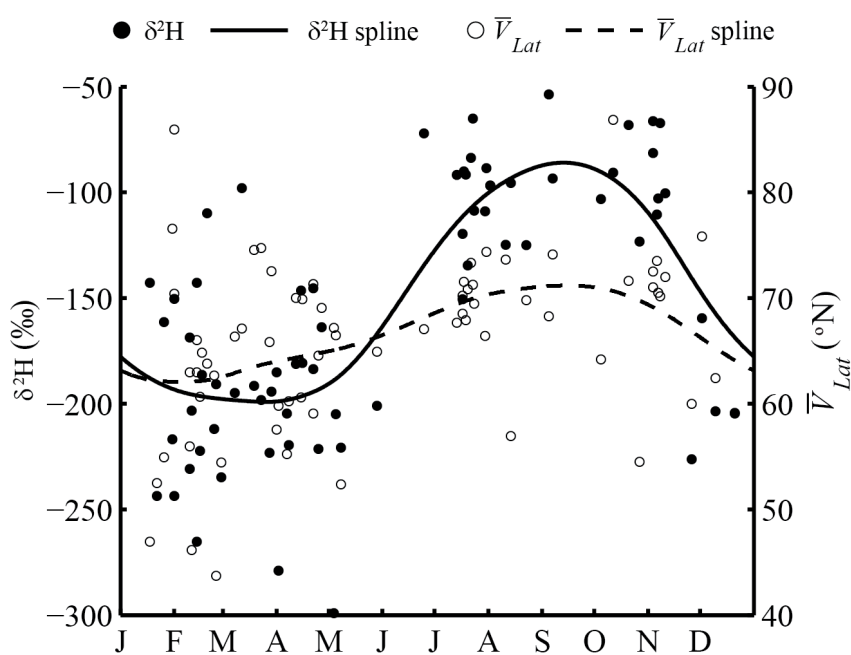
Figure 4. The measured δ^2H of Barrow precipitation and the mean latitude of the vapor source both exhibit an annual cycle and are in phase. The circles depict the raw data, while the lines are a spline fit to the data.
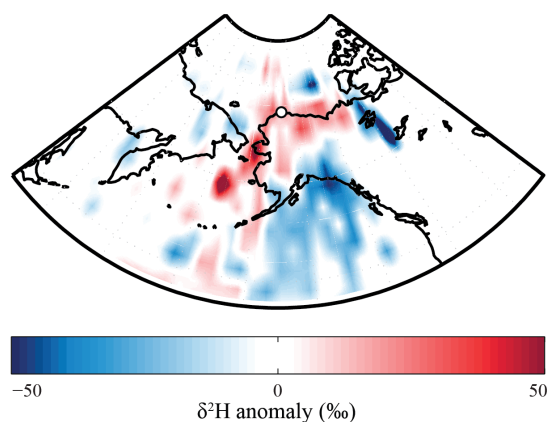
Figure 5. To demonstrate the effect of air parcel transport path, the δ^2H of precipitation with seasonal variation removed by subtracting the spline shown in Figure 4, is plotted at the vapor source. The data, which are on a 1 ° by 1 ° spatial scale, are smoothed for clarity. Vapor from the Bering Strait or Chukchi Sea tends to produce precipitation that is enriched relative to the average for that time of year. Likewise, vapor from the Gulf of Alaska tends to produce precipitation that is depleted relative to the average for that time of year. This variation in vapor source reflects a difference in transport path. Vapor originating from the Gulf of Alaska must rise to cross over the Alaska Range, inducing orographic precipitation and isotopic depletion relative to air masses that do not encounter orographic obstacles.
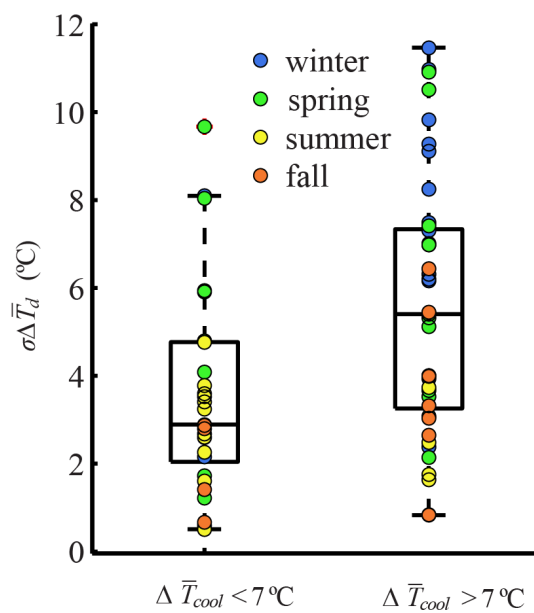
Figure 6. Distribution of standard deviations (σ) of $\bar{T}_d$ for events with $\Delta\bar{T}_{cool} < 7\,°C$ and $\Delta\bar{T}_{cool} > 7\,°C$. Colors indicate seasons. In general, small $\Delta\bar{T}_{cool}$ was associated with small $\sigma\bar{T}_d$. The variation in standard deviation is related to season, where warmer months tend to have smaller $\sigma\bar{T}_d$ and cooler months tend to have larger $\sigma\bar{T}_d$.

Atmospheric
Chemistry
and Physics
Discussions

Open Access
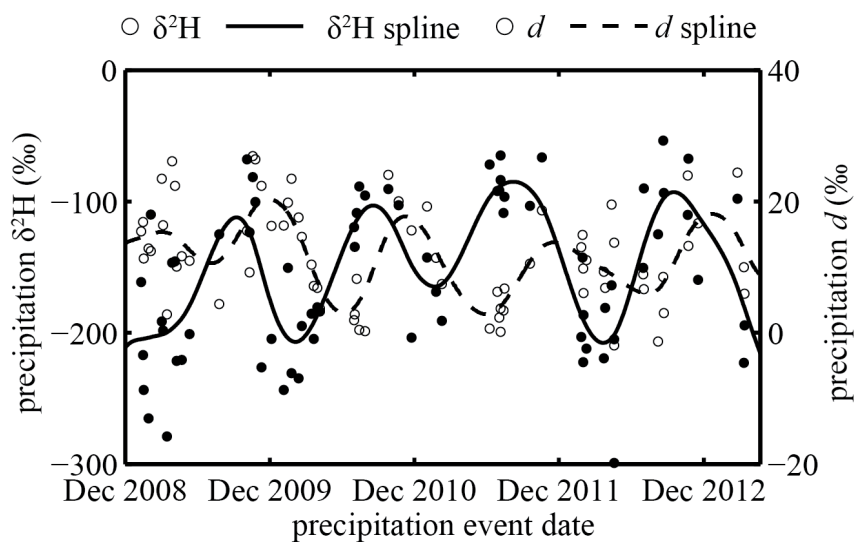
Figure 7. Annual maxima and minima in deuterium excess, d, lag those of $\delta^2 H$ by 2 - 3 months, such that the maximum is in fall and minimum in spring.

Atmospheric
Chemistry
and Physics

Discussions

Open Access

Table 1. Response variable: δ^2H, $R^2 = 0.52$. Variation in δ^2H is explained by air parcel cooling during transport ($\Delta \bar{T}_{cool}$), evaporation conditions ($\bar{T}_d$) and orographic obstacles in vapor transport path (mtn). The slope of the correlation is β. The variance estimate for each explanatory variable is calculated as square of the semi-partial correlation for that variable with δ^2H. The variances reported do not sum to the total variance explained because the explanatory variables are not perfectly orthogonal.

independent variable (units)	β ($\pm$ S.E.)	p-value	variance estimate
intercept	-96.9 (8.70)	< 0.001	
$\Delta \bar{T}_{cool}$ (°C)	-3.25 (0.58)	< 0.001	0.227
$\bar{T}_d$ (°C)	3.80 (0.78)	< 0.001	0.171
mtn (boolean)	-34.29 (11.05)	0.0028	0.069

Table 2. Response variable: δ^2H. Evaporation conditions ($\bar{T}_d$) explain variation in δ^2H for small $\Delta \bar{T}_{cool}$ while topographic highs below the trajectory (mtn) explain variation for large $\Delta \bar{T}_{cool}$. $\Delta \bar{T}_{cool}$ explains variability significantly for both subregions, but explains a third of the variance for the small $\Delta \bar{T}_{cool}$ subgroup.

Independent variable (units)	$\Delta \bar{T}_{cool} < 7\,°C$			$\Delta \bar{T}_{cool} > 7\,°C$		
	β ($\pm$ S.E.)	p-value	R^2	β ($\pm$ S.E.)	p-value	R^2
Intercept	-120.4 (8.01)	< 0.001		-127.0 (21.8)	< 0.001	
$\Delta \bar{T}_{cool}$ (°C)	-5.81 (1.87)	0.004	0.26	-2.84 (1.16)	0.019	0.13
Intercept	-109.1 (7.52)	< 0.001		-172.6 (9.60)	< 0.001	
$\bar{T}_d$ (°C)	3.9 (0.79)	< 0.001	0.48	3.77 (1.81)	0.038	0.10
Intercept	-124.7 (9.74)	< 0.001		-140.1 (13.2)	< 0.001	
mtn (boolean)	-21.5 (18.6)	0.26	0.05	-62.2 (17.6)	0.001	0.24

Table 3. Explaining Deuterium excess (d) with various metrics that quantify evaporation conditions. We show results from simple linear regressions with three different independent variables: evaporation site relative humidity ($\bar{h}_{2m}$), Sea surface temperature ($\bar{T}_{ss}$), and ($\bar{T}_{d}$). Relative humidity and sea surface temperature were explored independently because of correlation between the two.

Independent variable (units)	β ($\pm$ S.E.)	p-value	R^2
$\bar{h}_{2m}$ (%)	13.8 (15.0)	0.359	0.001
$\bar{T}_{ss}$ (°C)	-0.87 (0.35)	0.016	0.08
$\bar{T}_{d}$ (°C)	-0.53 (0.12)	< 0.001	0.24